Journal of Structural Biology 202 (2018) 82–93

Contents lists available at ScienceDirect

Journal of Structural Biology

journal homepage: www.elsevier.com/locate/yjsbi

Crystal structure of cystathionine β-synthase from honeybee *Apis mellifera*

Paula Giménez-Mascarell[a,1], Tomas Majtan[b,1], Iker Oyenarte[a], June Ereño-Orbea[a], Juraj Majtan[c], Jaroslav Klaudiny[d], Jan P. Kraus[b], Luis Alfonso Martínez-Cruz[a,*]

[a] Structural Biology Unit, Center for Cooperative Research in Biosciences (CIC Biogune), Technology Park of Bizkaia, 48160 Derio, Bizkaia, Spain
[b] Department of Pediatrics, School of Medicine, University of Colorado, Aurora, CO 80045, USA
[c] Laboratory of Apidology and Apitherapy, Institute of Molecular Biology, Slovak Academy of Sciences, Bratislava 84551, Slovakia
[d] Department of Glycobiology, Institute of Chemistry, Slovak Academy of Sciences, Bratislava 84538, Slovakia

ARTICLE INFO

Keywords:
CBS
Transsulfuration
Hydrogen sulfide
Homocystinuria
S-adenosylmethionine

ABSTRACT

Cystathionine β-synthase (CBS), the key enzyme in the transsulfuration pathway, links methionine metabolism to the biosynthesis of cellular redox controlling molecules. CBS catalyzes the pyridoxal-5′-phosphate-dependent condensation of serine and homocysteine to form cystathionine, which is subsequently converted into cysteine. Besides maintaining cellular sulfur amino acid homeostasis, CBS also catalyzes multiple hydrogen sulfide-generating reactions using cysteine and homocysteine as substrates. In mammals, CBS is activated by S-adenosylmethionine (AdoMet), where it can adopt two different conformations (basal and activated), but exists as a unique highly active species in fruit fly *Drosophila melanogaster*. Here we present the crystal structure of CBS from honeybey *Apis mellifera*, which shows a constitutively active dimeric species and let explain why the enzyme is not allosterically regulated by AdoMet. In addition, comparison of available CBS structures unveils a substrate-induced closure of the catalytic cavity, which in humans is affected by the AdoMet-dependent regulation and likely impaired by the homocystinuria causing mutation T191M.

1. Introduction

Transsulfuration is an ancient metabolic process that allows the interconversion of methionine (Met) and cysteine (Cys) through the common intermediates homocysteine (Hcy) and cystathionine (Cth) (Brosnan and Brosnan, 2006) (Fig. 1). In evolutionary terms, the transsulfuration consists in two routes, the "*reverse*" and the "*forward*" pathways (Carmel and Jacobsen, 2001). The reverse transsulfuration is found in a wide range of species, such as mammals and yeast, and converts Met into Cys (Brosnan and Brosnan, 2006) (Fig. 1). Some organisms, including enteric bacteria (Kredich, 1996; Auger et al., 2002), plants (Macnicol et al., 1981) and yeast (Cherest and Surdin-Kerjan, 1992), also possess the forward transsulfuration route that enables the formation of Met from Cys (Brosnan and Brosnan, 2006) (Fig. 1). Importantly, the presence or absence of these routes place different metabolic constraints on different organisms. For example, yeast can utilize either methionine or cysteine as a sulfur source, whereas humans are auxotrophic for Met, but are not for Cys.

Cystathionine β-synthase (CBS, EC 4.2.1.22), is the key enzyme in the reverse transsulfuration pathway (Mudd et al., 1965), and catalyzes the pyridoxal-5′-phosphate (PLP)-dependent condensation of serine and Hcy to form Cth and H_2O (Fig. 1). The following second step in the route is mediated by another PLP-requiring enzyme, the cystathionine-γ-lyase (CGL), that cleaves Cth into Cys, 2-oxobutyrate and ammonia (NH_3) (Banerjee et al., 2003; Miles and Kraus, 2004). The resulting Cys can either be used in protein synthesis or for the biosynthesis of glutathione (GSH, a potent antioxidant) (Beatty and Reed, 1980), taurine (an organic acid widely distributed in animal tissues and a major constituent of bile) (Stipanuk, 1986) or can be further catabolized into sulphate (Fig. 1) (Brosnan and Brosnan, 2006; Prudova et al., 2006). Thus, CBS links methionine metabolism to the biosynthesis of cellular redox controlling molecules (Mudd et al., 1982; Welch and Loscalzo, 1998; Seshadri et al., 2002; Meier et al., 2003; Beyer et al., 2004; Mudd, 2011). Because of its pivotal role in the transsulfuration pathway, lack of CBS activity leads to classical homocystinuria (CBSDH, Online Mendelian Inheritance in Man (OMIM no. 236200)), an autosomal

Abbreviations: CBS, cystathionine β-synthase; CBSDH, (CBS)-deficient homocystinuria; AdoMet, S-adenosyl-L-methionine; PLP, pyridoxal-5′-phosphate; AmCBS, cystathionine β-synthase from *Apis mellifera*; *d*CBS, cystathionine β-synthase from *Drosophila melanogaster* CBS; *h*CBS, cystathionine β-synthase from *Homo sapiens*; RnCBS, Rattus norvegicus CBS; MmCBS, Mus musculus CBS; ScCBS, Saccharomyces cerevisiae CBS; CeCBS, Caenorhabditis elegans CBS; TcCBS, Trypanosoma cruci CBS; *Eh*OASS, *Entamoeba histolytica* O-acetylserine sulhydrylase; OASTL, O-acetyl-L-serine(thiol)lyase; *Ec*TD, *Escherichia coli* threonine deaminase; *St*TS, *Salmonella typhimorium* tryptophan synthase

* Corresponding author.
E-mail address: amartinez@cicbiogune.es (L.A. Martínez-Cruz).
[1] These authors contributed equally to this work.

https://doi.org/10.1016/j.jsb.2017.12.008
Received 25 September 2017; Received in revised form 28 November 2017; Accepted 19 December 2017
Available online 21 December 2017
1047-8477/

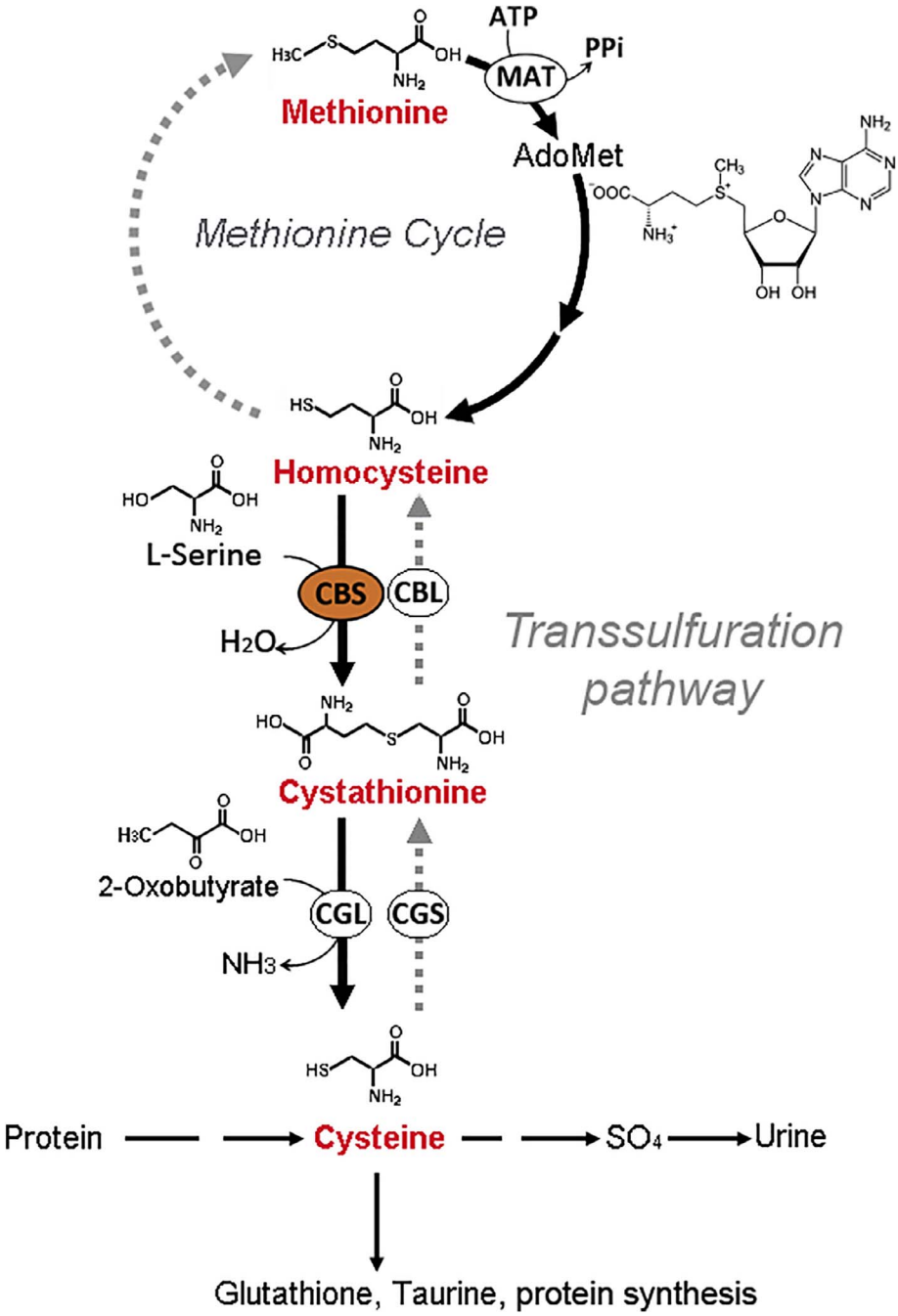

Fig. 1. The transsulfuration pathway. The *transsulfuration pathway*, the metabolic route that allows the conversion of homocysteine into cysteine, is connected to the *methionine cycle*. Cystathionine β-synthase (CBS) is the first enzyme in the reverse transsulfuration pathway (in black arrows), playing pivotal role in deciding the fate of homocysteine. In some organisms, such as bacteria and yeast, cysteine can be converted into homocysteine by the forward transsulfuration pathway (*grey* dashed arrows), which is mediated by the cystathionine γ-synthase (CGS) and cystathionine β-lyase (CBL) enzymes.

recessive inborn error of sulfur amino acid metabolism characterized by increased levels of Hcy in plasma and urine. Clinical symptoms of CBSDH manifest as a combination of connective tissue defects, skeletal deformities, vascular thrombosis, and mental retardation (Mudd et al., 2001). Remarkably, increased plasma Hcy concentrations are considered as a risk factor for dementia and Alzheimer's disease (Seshadri et al., 2002).

Besides maintaining cellular Hcy homeostasis, CBS also catalyzes alternative hydrogen sulfide (H_2S)-generating reactions using Cys and Hcy as substrates (Fig. S1) (Singh et al., 2009, 2011; Singh and Banerjee, 2011), what converts this enzyme in the major physiological source of hydrogen sulfide. H_2S plays a relevant role in the cardiovascular and nervous systems (Yadav and Banerjee, 2012; Paul and Snyder, 2012), induces smooth muscle relaxation, and has anti-inflammatory and cytoprotective effects on cells (Szabó, 2007). Noteworthy, alterations of the H_2S metabolism are linked with human diseases: in the brains of Alzheimer's disease patients H_2S synthesis is decreased (Eto et al., 2002), whereas in Down syndrome patients H_2S synthesis is increased due to the overexpression of CBS (Kamoun, 2004; Kabil and Banerjee, 2010). In turn, transsulfuration pathway-dependent H_2S production was found related to dietary restriction-mediated longevity in yeast, worm, fruit fly, and rodent models, providing an interesting explanation for the long-sought relationship between slimness and longevity (Hine et al., 2015).

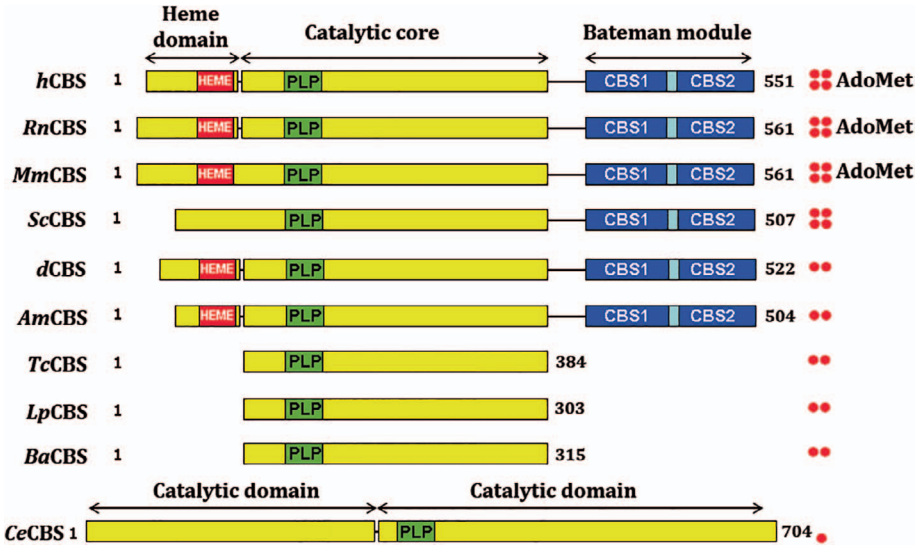

Fig. 2. The domain architecture, oligomerization and regulation of various CBS. In *yellow*, the catalytic domain (residues 1-386 in *h*CBS). The cofactors heme (*red*) and pyridoxal 5′-phosphate (PLP, *green*) bind to the heme domain and the catalytic core, respectively. The regulatory domain (Bateman module, *turquoise*) contains the CBS motifs pair (CBS1 and CBS2, *blue*). The total number of amino acids of the protein is also indicated. Red circles represent the most frequent oligomeric state: monomeric, dimeric or tetrameric. Abbreviations and Uniprot codes: *h*CBS, *Homo sapiens* CBS, P35520; *Rn*CBS, *Rattus norvegicus* CBS, P32232; *Mm*CBS, *Mus musculus* CBS, Q91WT9; *d*CBS, *Drosophila melanogaster* CBS, Q9VRD9; *Am*CBS, *Apis mellifera* CBS, Q2V0C9; *Sc*CBS, *Saccharomyces cerevisiae* CBS; *Ce*CBS, *Caenorhabditis elegans* CBS; *Tc*CBS, *Trypanosoma cruci* CBS, Q9BH24; *Lp*CBS, *Lactobacillus plantarum* CBS, F9UT54; *Ba*CBS, *Bacillus anthracis* CBS, Q81LL5.

The H_2S-production ability is not exclusive of eukaryotes but extends to bacteria as well, where the CBS and CGL genes are found clustered together (Matoba et al., 2017). Importantly, the presence of these genes is crucial for survival, as deletion of the CBS/CGL gene cluster or chemical inhibition of the encoded enzymes render pathogens such as *Bacillus anthracis*, *Lactobacillus plantarum*, *Helicobacter pylori* or *Pseudomonas aeruginosa* highly sensitive to a multitude of antibiotics (Shatalin et al., 2011).

The domain organization, quaternary structure and regulatory mechanism of CBS enzymes vary among species (Fig. 2). While most of the CBS enzymes form homotetramers like in humans (Ereño-Orbea et al., 2013a), rodents and yeasts (Jhee et al., 2000), we find homodimers in insects like fruit fly (Koutmos et al., 2010) or honeybee (Oyenarte et al., 2012), and monomers in worms (Vozdek et al., 2012) (Fig. 2). In higher eukaryotes, the N-terminal region includes a heme-binding domain (Fig. 2) that is thought to function in redox sensing and/or enzyme folding (Janosík et al., 2001b; Singh et al., 2007; Majtan et al., 2010). The heme-binding domain is followed by a conserved catalytic core with the fold of the type II family of PLP-dependent enzymes (Christen and Mehta, 2001; Meier et al., 2001). Finally, the C-terminal region, also known as "Bateman module", consists of two consecutive "CBS domains" (Fig. 2) (Bateman, 1997; Baykov et al., 2011; Ereño-Orbea et al., 2013b; Anashkin et al., 2017) and exhibits the highest degree of sequence variability in CBS primary structures (Vozdek et al., 2012). Strikingly, some organisms like *C. elegans* lack this module (Fig. 2), which plays a key role in regulating the activity and oligomerization degree of many CBS enzymes. Interestingly, the presence of missense mutations or the artificial removal of this region not only activates the human (Kery et al., 1998; Janosík et al., 2001a), and yeast (Taoka and Banerjee, 2002) CBS enzymes, but causes a disassembly of protein tetramers into homodimers (Meier et al., 2003; Kery et al., 1998). The molecular basis for all these observations has historically been delayed by the scarce availability of structural data, which until 2010 was limited to the catalytic core of human CBS (Meier et al., 2001; Taoka et al., 2002) and to the full-length enzyme from *Drosophila melanogaster* (Koutmos et al., 2010). The long-sought crystal structure of *h*CBS (Ereño-Orbea et al., 2013a, 2014; McCorvie et al., 2014) recently opened a new scenario and showed how, in the lack of the allosteric regulator S-adenosylmethionine (AdoMet), the Bateman module occludes the entrance to the catalytic cavity, thus maintaining the enzyme in a basal, low activity state (Fig. S2) (Ereño-Orbea et al., 2013a). It additionally revealed that binding of AdoMet to the Bateman module causes a relative rotation of its two CBS motifs that weakens their interaction with the loops configuring the entrance to the catalytic cavity, thus leading to the *activated* conformation of the enzyme (Fig. S2) (Ereño-Orbea et al., 2014). At the same time, Bateman modules from complementary subunits associate into an AdoMet-bound disk-like structure designated as *CBS module* that stabilizes an activated state (Ereño-Orbea et al., 2014) (Fig. S2). Such an activated state is structurally similar to that found in the fruit fly enzyme (Koutmos et al., 2010). Strikingly, the allosteric mechanism involving two different conformations (*basal* and *activated*) occurs only in mammals. CBS enzymes from less evolved eukaryotes, such as *Drosophila melanogaster*, only exist in a constitutively activated conformation ensuring a permanent access of substrates into the catalytic cavity (Koutmos et al., 2010).

Aimed to reduce the current structural gap existing in the CBS field, we describe herein the crystal structure of full-length CBS from honeybee *Apis mellifera* (*Am*CBS) at 3.2 Å resolution. These data provide new insights for understanding the molecular mechanisms involved in catalysis and allosteric regulation of CBSs, and may help to develop drugs to modulate CBS activity.

2. Results

2.1. Overall structure

The *Am*CBS crystals, grown as described previously (Oyenarte et al., 2012), belong to the space group $P2_12_12_1$ and contain two protein molecules in the asymmetric unit (Table 1). Each *Am*CBS subunit (Fig. 3) is composed of a (i) a N-terminal *heme domain* (residues 1-30); (ii) a central catalytic core (residues 31-343) and (iii) a C-terminal Bateman module (residues 371-504). The last two blocks are tethered by a long linker (residues 344-370) that contains two short α-helices (α11, α12) (Figs. 3, 4). Structurally, the fold of the catalytic core belongs to the β-family of the PLP-dependent enzymes and includes twelve α-helices and two β-sheets consisting of four (β3–β6) and six (β1–β2, and β7–β10) strands, respectively (Figs. 2 and 4).

Table 1
Statistics for data collection and refinement.

Protein construct	*Am*CBS
Data collection and Process	
Radiation source	Bruker Microstar H
Radiation wavelength (Å)	1.5418
Space group/ PDB code	$P2_12_12_1$/5OHX
a (Å)	86.1
b (Å)	96.1
c (Å)	180.7
Molecules per a.u.	2
Resolution (Å)	49.4–3.2 (3.3-3.2)
R_{sym} [a] (%)	15.4 (69.3)
Mean I/I	10.2 (2.6)
Completeness (%)	99.7 (99.9)
Redundancy	6.2 (5.8)
Wilson B factor (Å)	60.3
Refinement statistics	
Number of working reflections	25365
Number of test reflections	1287
R_{work} [b] (%)/R_{free} [c] (%)	19.7/23.1
No. of atoms	
Protein	7590
Ligand	116
Water	0
Average B factors (Å^2)	
Protein	60.035
Ligand	55.66
Water	0
RMSDs	
Bond lengths (Å)/angles (°)	0.003/1.128
Ramachandran plot statistics (%)	
Residues in most favored regions	96.7
Residues in additional allowed regions	3.3
Residues in disallowed regions	0

One crystal was used per data set. Values in parentheses are for the highest resolution shell. [a]$R_{sym} = \Sigma_{hkl}\ \Sigma_i\ |I_i\ (hkl) - \langle I(hkl)\rangle I/\Sigma_{hkl}\ \Sigma_i\ I_i(hkl)$; [b]$R_{work} = \Sigma\ |F_o - F_c\ |/\Sigma F_o$; [c]$R_{free} = \Sigma\ |F_o - F_c|/\Sigma F_o$, calculated using a random 5% of reflections that were not included throughout refinement. N/A, not applicable.

2.2. The heme domain

The heme binding domain of *Am*CBS is ten and forty residues shorter than the equivalent region in *d*CBS (Koutmos et al., 2010) and *h*CBS (Meier et al., 2001; Taoka et al., 2002) (Ereño-Orbea et al., 2013a; McCorvie et al., 2014), respectively (Fig. 4). It lacks secondary elements and embraces three helices of the catalytic core (α3, residues 77-92; α7, residues 185-202 and α8, residues 218-230) (Fig. S3). Its function remains enigmatic but the sequence and structural similarity with *h*CBS suggest that it likely fulfills a structural and/or a regulatory role (Taoka et al., 2002; Janosík et al., 2001a; Majtan et al., 2008; Weeks et al., 2009). The heme group is relatively surface exposed and is nested in a hydrophobic pocket formed by residues 7-24, helices α7 and α8 and the loop following the strand β6 (Figs. 4, S3). The iron in heme is axially coordinated by the sulfhydryl group of Cys12 and the $N_{\varepsilon 2}$ atom of His23. In turn, the sulfhydryl group of Cys12 forms additional polar interactions with the side chain of Arg225 and the main chain nitrogen of Trp14 (Fig. S3). The heme carboxylate groups are partially solvent accessible and participate in polar interactions with other residues like Arg8 or Tyr11.

2.3. The catalytic core

The central catalytic core of *Am*CBS (Fig. 3) is structurally similar to that found in the human (Meier et al., 2001; Taoka et al., 2002; Ereño-Orbea et al., 2013a, 2014; McCorvie et al., 2014) and in the fruit fly (Koutmos et al., 2010) CBSs, and shows the overall fold of PLP-dependent enzymes (Fig. S4). Interestingly, the comparative analysis of all these enzymes revealed that this region is in turn composed by two distinguishable blocks: (i) a large *static* subdomain that in *Am*CBS includes amino acid residues 1-76 and 184-342 (Fig. 4) (the equivalent residues in *h*CBS are 1-116 and 226-384, respectively; see Fig. S5) and (ii) a small *moveable* subdomain, which is intercalated in the larger block and includes residues 77-183 and 117-225 in *Am*CBS and *h*CBS, respectively (Fig. 4, S5). Both subdomains present an α/β fold and are linked in *Am*CBS by two loops formed by residues 70-77, that link strand β2 and helix α3, and 279-284, that are located between strand β6 and helix α7 (Fig. 4). The crevice formed between the *static* and the *moveable* subdomains (Fig. S4) accommodates the PLP cofactor, which is deeply buried in the cavity and resides as an internal aldimine, where the ε-amino group of Lys78 forms a Schiff base with aldehyde of PLP (Fig. S3). There are other hydrogen bonds between the nitrogen of the pyridine ring and the O_γ of Ser307, and between the 3′-hydroxyl group of PLP and the $N_{\delta 2}$ of Asn108. A highly conserved phosphate binding loop known to participate in catalysis and composed by residues Gly215, Thr216, Gly217, Gly218 and Thr219 in *Am*CBS, is located between strand β7 and helix α8 (Figs. S3 and S5). In *Am*CBS, the

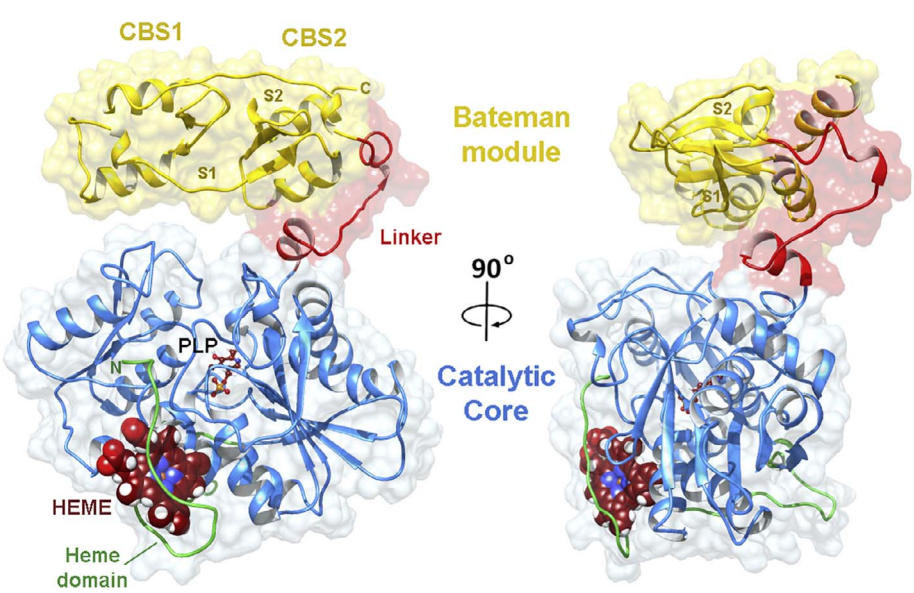

Fig. 3. Structure of the *Am*CBS protomer. The N-terminal domain (in *green*) with heme cofactor (spheres) precedes the catalytic core (in *blue*) that contains the PLP molecule (balls and sticks) at the catalytic site. The C-terminal Bateman module (in *yellow*) includes two CBS motifs (CBS1, CBS2) and is linked to the core through a long linker (in *red*). Two main (empty) cavities, S1 and S2, are formed between the central β-sheets of the two CBS motifs.

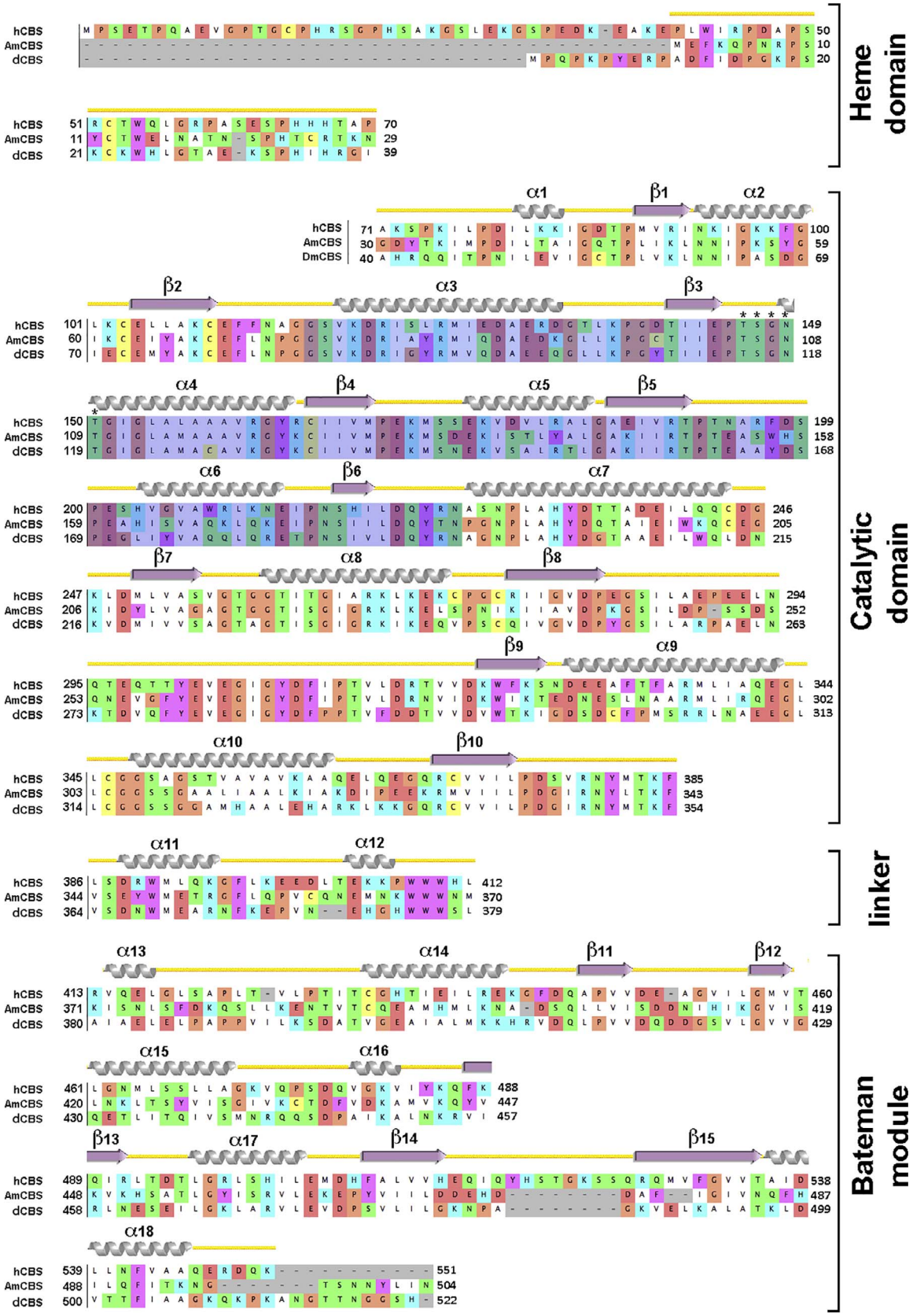

Fig. 4. CBSs sequences. Sequence alignment of full-length cystathionine β-synthases from *Homo sapiens* (*h*CBS, Uniprot code P35520), *Apis mellifera* (*Am*CBS, Uniprot Q2V0C9) and *Drosophila melanogaster* (*d*CBS, Uniprot Q9VRD9). The *moveable* subdomain of the catalytic core is shadowed in *blue*. The secondary elements of *Am*CBS are indicated.

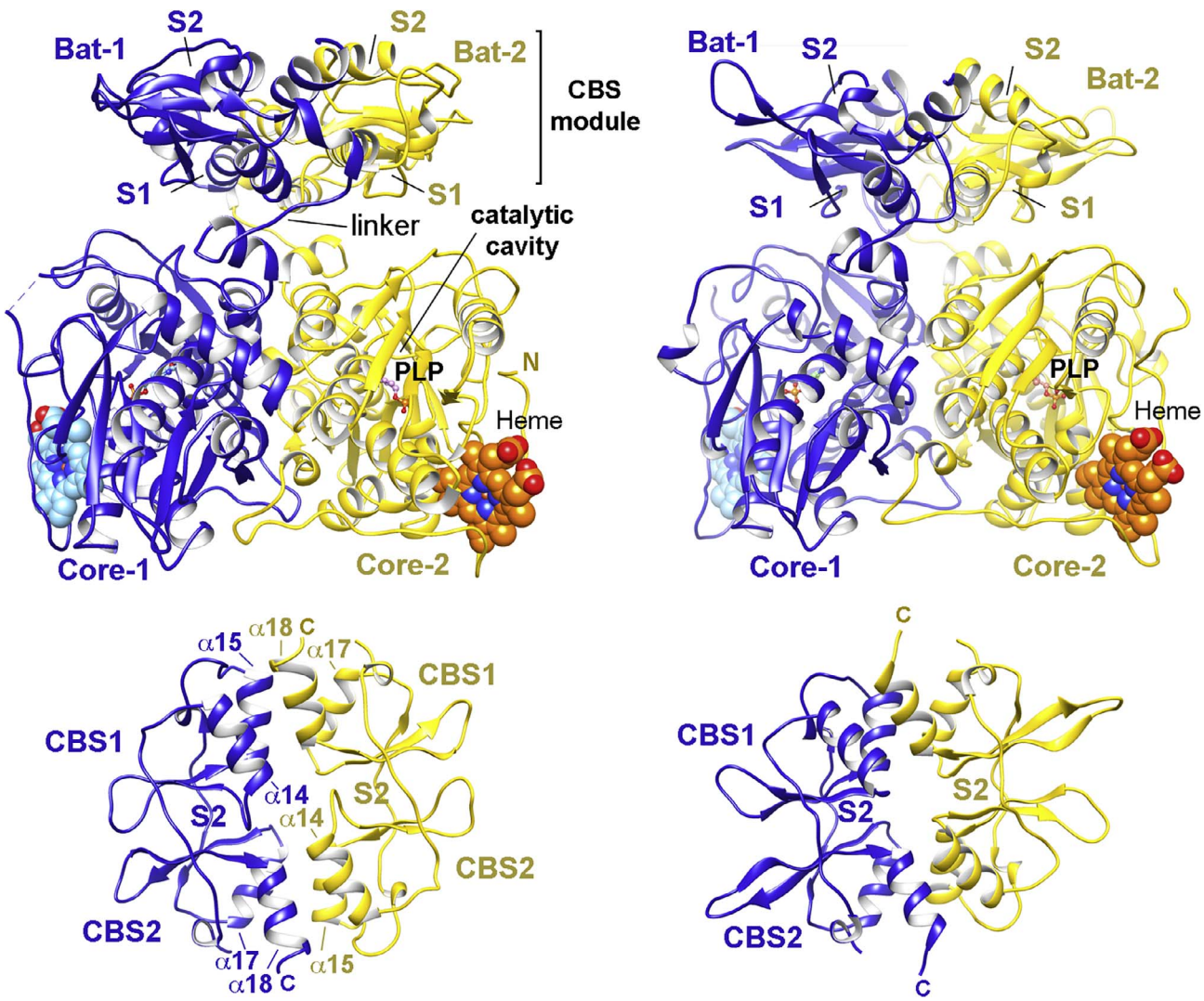

Fig. 5. Structure of the *Am*CBS dimer. *Am*CBS (*left*) exists as a tight dimer in which the two protomers interact through residues located at both, the catalytic and the regulatory region similarly to *d*CBS (*right*) (Koutmos et al., 2010). In both proteins, the Bateman modules (Bat-1 and Bat-2) from complementary subunits associate into a disk-like *CBS module*. In this conformation, the entrance to the catalytic cavity of each subunit is open and accessible, thus yielding a highly active species. Each Bateman module contains two cavities (S1 and S2) that, in contrast with the human enzyme, are not able to bind AdoMet. Heme and PLP are depicted in spheres and sticks, respectively.

entrance of the catalytic cavity is defined by four loops that include residues 104-107, 128-134, 151-161 and 253-274. The first three loops are located in the *moveable* subdomain, while the fourth loop belongs to the larger *static* subdomain. In our *Am*CBS crystals, residues 252-254 of the fourth loop are not visible in the electron density map, suggesting a high mobility of this zone in the absence of bound substrates, as it has previously been described in both *h*CBS (Meier et al., 2001) and *d*CBS (Koutmos et al., 2010).

2.4. The Bateman module of AmCBS does not host AdoMet

The Bateman module within the C-terminal domain is tethered to the catalytic core by a long linker (residues 341-370) (Figs. 3 and 5) and consists of two CBS motifs (CBS1: 369-430; CBS2: 437-504) that exhibit a α13-α14-β11-β12-α15 and a α16-β13-α17-β14-β15-α18 fold, respectively (Figs. 3-5). Each short N-terminal helix (α13 or α16) forms an integral part of the other CBS motif by antiparallel packing between its C-terminal β-strand (β12 or β15) and the α-helix (α18 or α15), so that both CBS motifs form a nested structure with pseudo-C_2 symmetry (Fig. 5). The two CBS motifs interact with each other via their two- or three-stranded β-sheets, and both long edges of this bilayer interface form two major cavities (designated S1 and S2) (Figs. 4 and 5). Importantly, the chemical-physical properties of sites S1 and S2 lack key features to host nucleotides thus explaining why, in contrast with mammals, insect CBS enzymes do not bid and are not regulated by AdoMet. Among these features is, for example, the lack of a conserved aspartate at the first turn of the α-helix following the last β-strand of each CBS domain (Figs. 6, S6), which is crucial to stabilize the orientation of the ribose ring of the nucleotide within the cavity through the interaction with its hydroxyl groups (Ereño-Orbea et al., 2013a,b, 2014). In *Am*CBS, the position of this aspartate is occupied by a lysine (K422) or by a histidine (H487) in sites S1 and S2, respectively (Figs. 6, S6). In addition, the hydrophobic cage required to accommodate the adenine ring of the nucleotide (Ereño-Orbea et al., 2013b; Baykov et al., 2011; Anashkin et al., 2017) is only partially present in site S1 (residues Y467, V443, V447, V468) and is completely absent in cavity S2, which

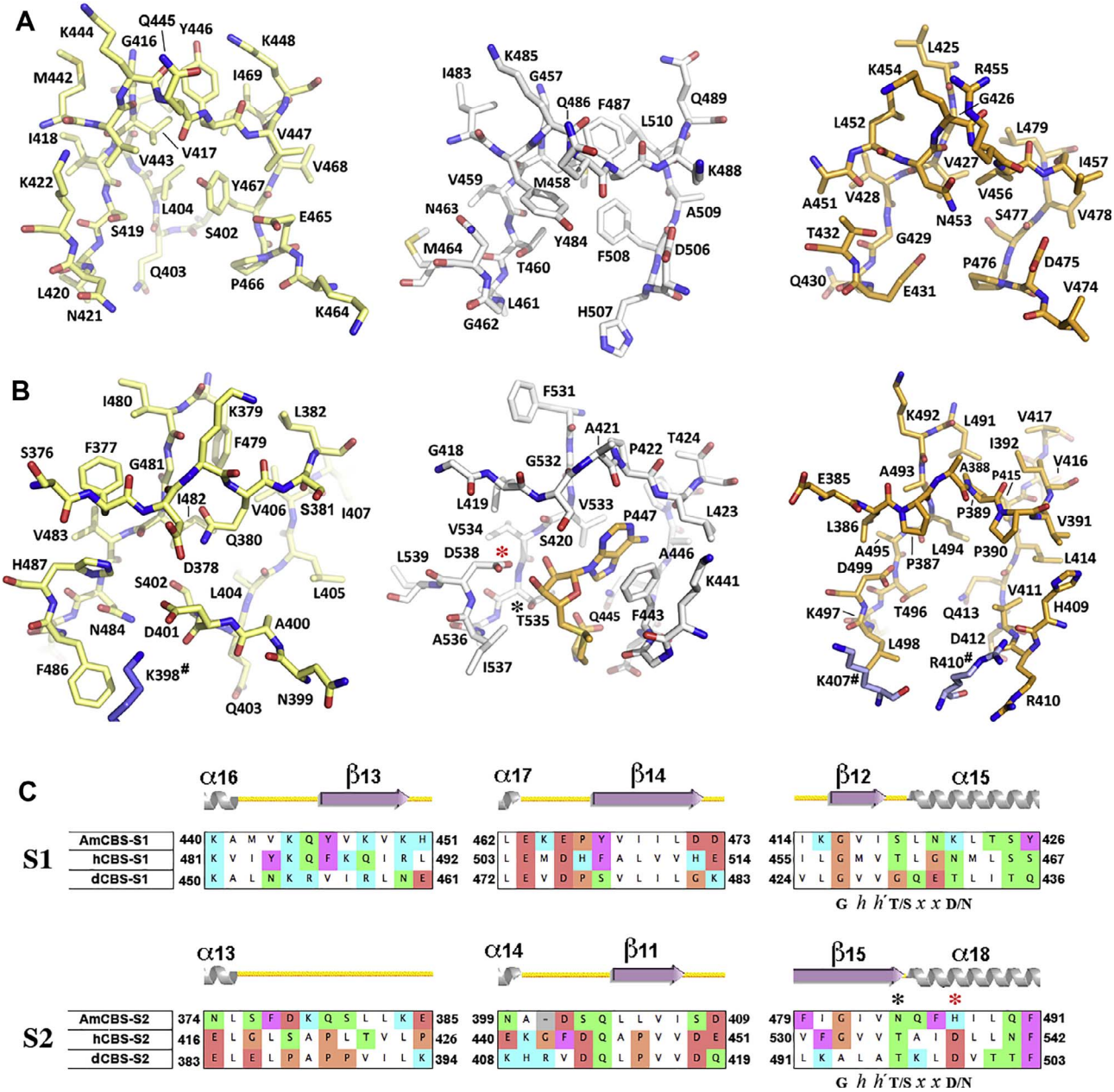

Fig. 6. Sites S1 and S2 in *Am*CBS, *h*CBS and *d*CBS. The figure shows the main residues located at (A) site S1 and (B) site S2 of *Am*CBS (left, in *yellow*), *h*CBS (middle, in *grey*) and *d*CBS (right, in *orange*), respectively. AdoMet at site S2 of *h*CBS is represented in *orange* sticks. Residues from complementary subunits are in *blue* sticks, indicated with #. The presence of an aspartate residue as well as of a threonine at the equivalent position of residues D538 and T535 of *h*CBS (marked in panels B and C with *red* and *black* asterisks, respectively), is a known key feature to host adenosine derivatives in the canonical cavities of CBS domains (Baykov et al., 2011; Ereño-Orbea et al., 2013b) (Supp. Fig. S6). (C) Sequence alignment of the main amino acid residues configuring the walls of sites S1 and S2 in *Am*CBS, *h*CBS and *d*CBS. The nucleotide binding motif G-*h*-*h*-T/S-*x*-*x*-D/N usually found in CBS domains that host adenosine derivatives (where "*h*" is hydrophobic, "*x*" is any residue, T/S is a threonine or a serine residue and D/N is an aspartate /asparagine residue) (Ereño-Orbea et al., 2013b) (see also Supp. Fig. S6), is indicated underneath the third block of aligned residues. The secondary elements that contain the corresponding residues in *Am*CBS are indicated above the alignment.

is occupied by polar residues (N484, N399, D401, S402, Q403) (Fig. 6). Similar characteristics can be observed in *d*CBS (Koutmos et al., 2010) (Fig. 6), which has very high basal activity (Fig. S7) (i.e. is constitutively active) and does not bind nor is regulated by AdoMet (Majtan et al., 2014).

Of note, the Bateman module of *Am*CBS does not contact the catalytic core except via the connecting linker (Figs. 3 and 5, Movie S1). This arrangement helps maintaining a concrete distance between the CBS2 motif of the Bateman module and the loops defining the entrance of the active site cavity. The CBS1 motif also remains far apart from the protein core with no elements in between (Fig. 3). Among the main interactions between the linker and the CBS2 domain is a salt link between residues E350 (at helix α11) and R460 (at helix α17). The position of the α-helical region of the linker is supported by hydrophobic interactions between Y347 (α11) and the alkyl chains of residues R460 (at helix α17) and K464. The linker maintains several hydrophobic interactions with the catalytic core through residues M349 (α11), I336, Y339, F343, V344, L355, and R294 (α9), I297 (α9) and L303.

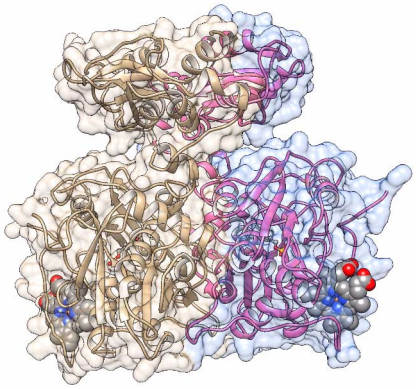

Movie S1. Similarly to *d*CBS (Koutmos et al., 2010), *Am*CBS associates into tight dimers that represent the functional biological unit. Each subunit shares a large interface (3282 Å^2) with the complementary subunit with extensive contributions from the central core (1861 Å^2) and the Bateman module (1316 Å^2) (Fig. 5). This interface is mainly hydrophobic with hydrogen bonds and no salt bridges between the two protomers. A pair of four-helix bundles forms the interface (α14 and α15 from CBS1 of protomer A interact with α17 and α18 from CBS2 of protomer B, and α17 and α18 from CBS2 of protomer A with α14 and α15 from CBS1 of protomer B) (Fig. 5). Remarkably, the two Bateman modules from the complementary subunits associate through their helix bundles to configure an antiparallel disk-like *CBS module* (Fig. 5) (Baykov et al., 2011; Ereño-Orbea et al., 2013b; Anashkin et al., 2017). Such arrangement is rare among CBS domain proteins as Bateman modules usually associate into parallel CBS modules; however, it is observed in structures of all full-length CBS enzymes solved so far (Koutmos et al., 2010; Ereño-Orbea et al., 2014). It imposes a physical separation between the Bateman module and the entrance of the catalytic cavity and permits free access of substrates into the catalytic site (Fig. 5). Thus, our crystals contain constitutively active dimers of *Am*CBS.

3. Discussion

The crystal structure of *Am*CBS described herein provides the third three-dimensional structure of a full-length CBS enzyme (second from an insect) containing a regulatory Bateman domain available to date. Two additional structures of full-length CBS enzymes from *Lactobacillus plantarum* (PDB code 5BIH) (Matoba et al., 2017) and from *Bacillus anthracis* (PDB code 5XW3) (Devi et al., 2017) have been deposited recently, although the corresponding protomers do not include a Bateman module in their amino acid sequences (Fig. 2). The species present in our crystals correspond to highly active dimers (likely constitutively activated), (Fig. 5, Movie S1). Similar conformation and consequences have also been observed for *d*CBS (Koutmos et al., 2010; Majtan et al., 2014). The main cavities (S1 and S2) in the Bateman module of *Am*CBS lack key residues and characteristics usually required to host nucleotides or their structural analogs, as shown for the human enzyme (Ereño-Orbea et al., 2014; McCorvie et al., 2014) and other CBS domain proteins of unrelated function (Baykov et al., 2011; Ereño-Orbea et al., 2013b) (Figs. 6, S6). Therefore, AdoMet, the allosteric activator of the mammalian enzyme (Ereño-Orbea et al., 2014; McCorvie et al., 2014), cannot bind and consequently does not regulate the *Am*CBS activity (Fig. S7). It seems clear that the capability of CBS to adopt two different conformations, the basal (of low activity) and the activated, is exclusive to mammals and appeared later in evolution (Kabil et al., 2011).

The structural data on CBS enzymes obtained during the last decade (Meier et al., 2001; Taoka et al., 2002; Koutmos et al., 2010; Ereño-Orbea et al., 2013a, 2014; McCorvie et al., 2014; Matoba et al., 2017) revealed a significant resemblance between the catalytic core of CBSs and the β-family of PLP-dependent enzymes (Fig. S4). However, the difficulties found to crystallize full-length CBS enzymes in the absence and in the presence of their multiple ligands have prevented to prove with certainty whether CBSs suffer substrate-induce conformational changes analogous to those reported for the related PLP-dependent enzymes (Raj et al., 2013). For example, binding of methionine to conserved residues surrounding the active site of O-acetyl serine sulfhydrylase (OASS) (evolutionary the most closely related PLP-dependent enzyme to CBS) results in the movement of the N-terminal domain and the closure of the active site (Raj et al., 2013). Similar changes were observed in threonine deaminase (TD) (Hyde et al., 1988) or tryptophan synthase (TS) (Rhee et al., 1996). By analyzing all the available structural information on CBS enzymes, we found that the *moveable* subdomain of CBS catalytic core participates in such substrate-induced structural change (Fig. 7). Of note, in OASS the majority of the substrate-to-protein hydrogen bonding interactions affect the residues located in two conserved loops: the "*Asn loop*" (85-TSGNT-89) from the N-terminal domain and the "*Gly loop*" (236-GIGA-239) from the C-terminal domain (marked with asterisks in Fig. S5). In this protein, the largest conformational change observed in the substrate-bound state is represented by residue S86 (equivalent to S106 in *Am*CBS and S147 in *h*CBS), which shifts around 6 Å to make contacts with the substrate methionine in the active site (Raj et al., 2013). Although it has not been credited as important as the Asn loop, some additional elements including strands β4 to β7, helices α6, α7 and loops 85-88 and 130-133 of OASS (all belonging to the small subdomain), modify their conformation concomitantly (Raj et al., 2013). Our comparative analysis (Fig. S5) shows that CBS enzymes contain equivalent loops in their amino acid chains represented by 105-TSGNT-109 (Asn loop) and 263-GIG-265 (Gly loop) in *Am*CBS, by 146-TSGNT-150 and 305-GIG-307 in *h*CBS, and by 115-TSGNT-119 and 274-GIG-276 in *d*CBS, respectively (Figs. 4, S5). Noteworthy, the structural superimposition of basal *h*CBS (PDB codes 4L3V, 4L0D) (Ereño-Orbea et al., 2013a) with AdoMet-bound activated *h*CBS (PDB code 4PCU) (Ereño-Orbea et al., 2014) also revealed that strands β4 to β7, loops L171-174 and L191-202, as well as helices α6 and α7 (comprising a major part of the *moveable* subdomain), vary their orientation in the activated state with respect to the basal conformation (Fig. 7). Of note, we have noticed that helices α4 and α5 of *h*CBS remain unaltered and anchor the *moveable* motif to the *static* subdomain. These observations indicate that the inhibitory effect exerted by the regulatory Bateman module of *h*CBS in the basal state (Ereño-Orbea et al., 2013a) is not determined solely by a closure of the loops defining the entrance of the catalytic cavity, as we initially thought (Ereño-Orbea et al., 2014), but by the compression of a major part of the *moveable* subdomain of the protein core that behaves as rigid body. Moreover, an equivalent whole-motif displacement is observed in *d*CBS when the structure of the native protein (PDB ID 3PC3) is superimposed with its corresponding substrates-bound complexes (PDB codes 3PC3, 3PC4) (Koutmos et al., 2010). As shown in Figs. 7 and 8, binding of substrates into the catalytic cavity of *d*CBS promotes the movement of the entire *moveable* motif, and not of just the entrance loops, as was formerly proposed (Koutmos et al., 2010). In the same way, it can be shown that the effect of substrate binding in OASS is not limited to the displacement of a single loop (Raj et al., 2013), but involves a shift of a region equivalent to the *moveable* motif of *h*CBS (Fig. 7). Based on these observations and despite no crystal structure of *h*CBS in complex with its substrates is available so far, it is reasonable to postulate that there are two circumstances that trigger a displacement of the *moveable* motif and the consequent closure of the catalytic cavity in the human enzyme: (i) the presence of the Bateman module above the catalytic cavity (as seen in the basal state) and (ii) the presence of bound substrates at the PLP site. Interestingly, in constitutively active CBS enzymes, such as *d*CBS or *Am*CBS, where the Bateman module never interacts with the catalytic core, the closure of the *moveable* motif appears to exclusively dependent on the presence of bound substrates

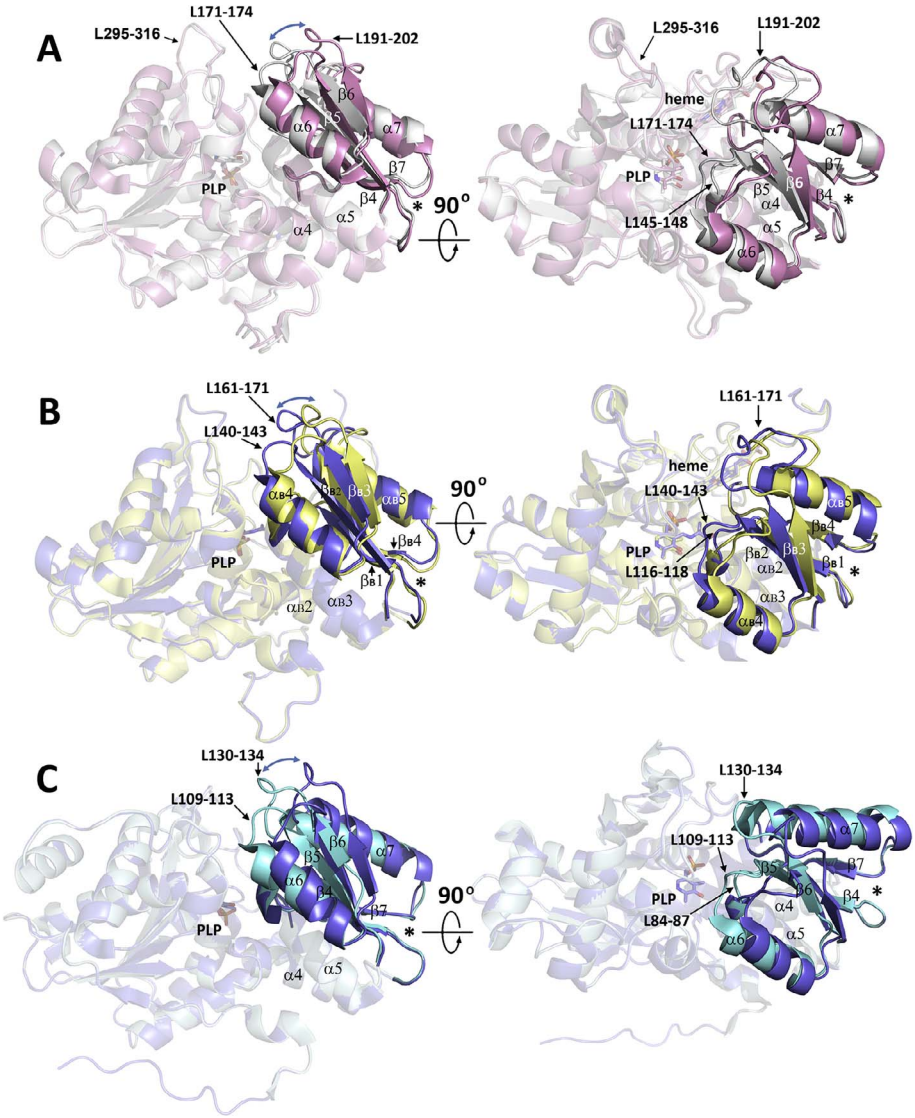

Fig. 7. The *moveable* subdomain in PLP enzymes. (A) Structure of the *basal* (*grey*, PDB ID 4LOD) and *activated* (*pink*, PDB ID 4PCU) conformation of the catalytic core of *h*CBS. In the *basal* state, the *moveable* submotif remains in a closed conformation (in *grey*) due to the presence of the Bateman module (not shown) above the catalytic cavity. Binding of AdoMet at the Bateman module triggers a migration of the latter from atop the catalytic cavity, thus allowing the displacement of the *moveable* motif towards an open conformation (*pink*). The shift is indicated with a blue arrow. Although not represented, the artificial removal of the Bateman module (Meier et al., 2001) exerts a similar effect in *h*CBS, and facilitates the aperture of the *moveable* motif. (B, C) In the absence of substrates in the catalytic cavity, the *moveable* subdomain of (B) *d*CBS; (PDB ID 3PC2) and (C) *Eh*OASS (PDB ID 2PQM), adopts an open conformation (in *yellow* and *blue slate*, respectively) that evolves towards a closed state (PDB IDs 3PC4 in *blue marine* and 3BM5 in *cyan*, in B and C, respectively), when the substrates enter the PLP cavity.

inside the catalytic cavity. In agreement with this hypothesis, the *moveable* motif of *Am*CBS shows an open state in our crystals equivalent to that found in apo-*d*CBS (PDB code 3PC2) (Koutmos et al., 2010) (Fig. 8).

Interestingly, twelve of the 160 pathogenic mutations described in homocystinutic patients (http://cbs.lf1.cuni.cz/mutations.php) affect residues that are located in the *moveable* submotif (Fig. 9). This group includes the mutation T191M that is prevalent in the Iberian Peninsula and South America, (Urreizti et al., 2003, 2006a,b; De Lucca and Casique, 2004; Porto et al., 2005; Bermúdez et al., 2006; Hnízda et al., 2012; Alcaide et al., 2015). The T191M variant is structurally unstable and shows decreased catalytic activity and higher susceptibility to an accelerated proteasome-dependent degradation (Hnízda et al., 2012). Several explanations have been proposed over the years for the effect of the T191M mutation on the *h*CBS activity (Katsushima et al., 2006; Urreizti et al., 2003, 2006a,b). Urreizti et al. speculated that mutation T191M might interfered with the normal substrate-induced mobility of the region 186-222 making it impossible for the *h*CBS to retain PLP within the catalytic cavity (Urreizti et al., 2003, 2006a,b). In light of our recent structural data (Ereño-Orbea et al., 2013a, 2014), it is reasonable to think that this mutation likely imposes a steric hindrance that severely distorts its environment (Fig. 9), thus impairing the entire three-dimensional fold of the *moveable* subdomain and consequently the conformational change associated with the aperture of the catalytic cavity. This would explain the structural instability and extensive unfolding caused by the mutation T191M (Hnízda et al., 2012), in both the basal and activated states of *h*CBS. We hypothesize that a similar scenario might occur in mutants V168M, I143M and E144K, which are also located in this región (Fig. 9).

The structural data presented herein represents another step towards understanding the molecular mechanism underlying the catalysis and regulation of the CBS enzymes. Together with previously elucidated molecular mechanism of allosteric regulation of CBS by AdoMet (Ereño-Orbea et al., 2013a, 2014; McCorvie et al., 2014), herein described substrate-induced closure of the catalytic site broadens our knowledge and both will be instrumental in the rational design of drugs modulating CBS activity.

Author contributions

PG-M, IO, JE-O and LAMC performed structural analyses. TM subcloned and purified *Am*CBS. JM and JK provided honeybee cDNA. TM, JPK and LAM-C conceived the idea of the project and provided all resources and funding. LAM-C wrote the initial draft and prepared figures. All authors read, revised and approved the final versión of the manuscript.

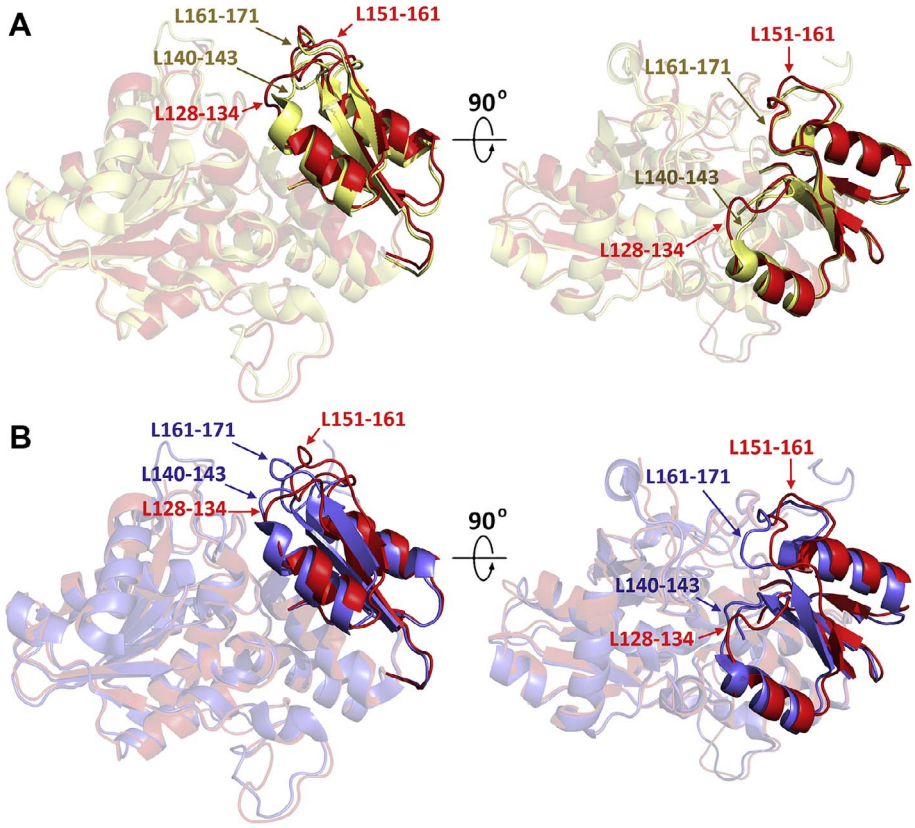

Fig. 8. Substrate-induced closure of the catalytic cavity. Structural superimposition of the catalytic core of *Am*CBS (*red*) with the catalytic core of (A) apo-*d*CBS (*yellow*, PDB ID 3PC2) and (B) *d*CBS with bound aminoacrylate (*blue* PDB ID 3PC3) or with serine (3PC4, not represented). The loops (and residues) involved in configuring the entrance to the catalytic cavity are indicated with arrows. The *moveable* submotif is enhanced in solid ribbons, whereas the *static* domain is in transparent cartoon.

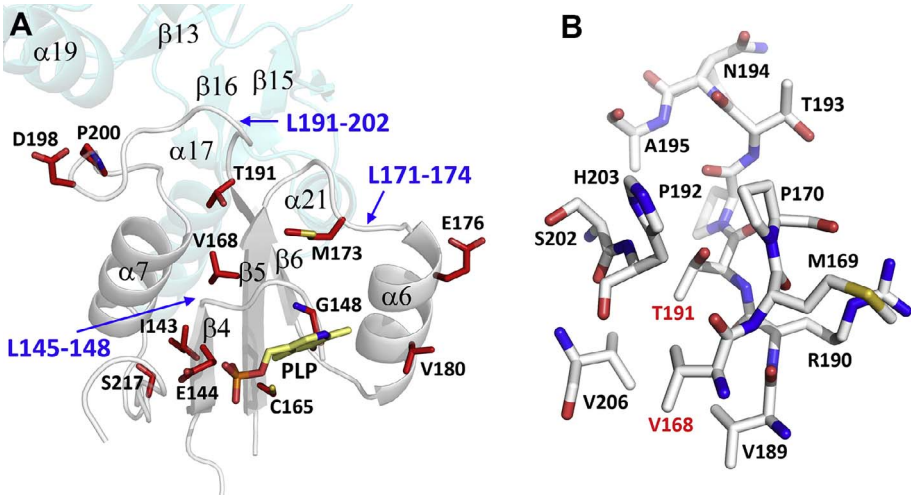

Fig. 9. Pathogenic mutations located in the *moveable* submotif of *h*CBS. (A) The pathogenic mutations located in the *moveable* motif (the affected residues are in *red*) are distributed in the three main loops (L145-148, L171-174 and L191-202) determining the access of substrates into the catalytic cavity of *h*CBS (e.g. G148R, M173V, T191M, D198V, P200L) or in the vicinity of these loops. The Bateman module above the entrance of the PLP site is represented in cyan. (B) Residues T191 and V168 are surrounded by hydrophobic residues including M169, P170, V189, P192, A195, H203 and V206.

Materials and Methods

Expression and purification of AmCBS

The pET-28a-C-*Am*CBS expression construct was prepared as described previously (Oyenarte et al., 2012). Full-length *Am*CBS was expressed and purified following the protocols that were developed for other CBS enzymes (Oyenarte et al., 2012).

Crystallization, X-ray diffraction data collection, phasing, and refinement

Crystals of *Am*CBS were obtained by the hanging-drop vapor diffusion method at 293 K in 24-well VDX crystallization plates according to the protocol described previously (Oyenarte et al., 2012). Drops consisted of 0.5 μL protein solution mixed with 0.5 μL precipitant solution (10% PEG 6000, 0.1 M HEPES-NaOH pH 7.5, 5% (±)-2-methyl-2,4-pentanediol) equilibrated over a reservoir volume of 0.5 mL; the protein concentration was 6 mg mL^{-1}. Single-crystals were cryoprotected with 25% (±)-2-methyl-2,4-pentanediol and flash frozen in liquid nitrogen. *Am*CBS data sets were collected at our in-house X-ray platform using a MAR345 detector mounted on a Microstar-H rotating-anode X-ray generator (Bruker), operated at 60 kV and 100 mA, with optics Helios and copper target (Cu Kα; λ = 1.542 Å). The difficulties found to grow suitable crystals prevented a subsequent data at Synchrotron Facilities. Data were processed using the software HKL2000 (Otwinowski and Minor, 1997) or XDS (Kabsch, 2010).

The *Am*CBS structure was determined by molecular replacement with the program PHENIX (Adams et al., 2010), using the crystal

structure of the *d*CBS (PDB 3PC2) as the initial search model. Crystallographic refinement was carried out with PHENIX (Adams et al., 2010) and REFMAC5 (Winn et al., 2003; Murshudov et al., 2011). Ramachandran statistics for the refined coordinates (residues in favored region (%), number of outliers) were (97.27%, 0.11) for *Am*CBS. The final refinement statistics are summarized in Table 1.

The structural analysis of all enzymes discussed in this manuscript was done using The PyMOL Molecular Graphics System (http://www.pymol.org) and Coot (Emsley et al., 2010). Calculation of surfaces was done with the PISA server (Krissinel and Henrick, 2007). The figures showing three-dimensional protein structures were prepared with PyMOL and CHIMERA (http://www.rbvi.ucsf.edu/chimera) (Pettersen et al., 2004). Sequence alignments were done with Clustal W (Larkin et al., 2007) and represented with CINEMA (Parry-Smith et al., 1998).

CBS specific activity measurements

The CBS activity in the classical reaction was determined by a radioisotope assay using (^{14}C(U)) L-serine as the labeled substrate, essentially as described previously (Majtan et al., 2010).

Accession numbers

The atomic coordinates of *Am*CBS, and structure factors reported in this paper have been deposited in the Protein Data Bank database, under PDB ID code 5OHX.

Availability of supporting data

The crystal structures used in the analysis are available in the Worldwide Protein Databank (http://www.wwpdb.org) under PDB IDs: *Apis mellifera* CBS (*Am*CBS): 5OHX; *Homo sapiens* CBS (*h*CBS): 4L3V, 4L0D, 4L28, 4L27, 4PCU, 4COO, 1M54, 1JBQ; *Drosophila melanogaster* CBS (*d*CBS): 3PC2, 3PC3, 3PC4; *Entamoeba histolytica* O-acetylserine sulhydrylase (*Eh*OASS): 2PQM, 3BM5, 4JBL, 4IL5, 4JBN; O-acetyl-L-serine(thiol)lyase (OASTL); *Escherichia coli* threonine deaminase (*Ec*TD): 1TDJ and *Salmonella typhimorium* tryptophan synthase (*St*TS): 1BKS, 2J9X.

Funding

This work was supported by a Scientist Development Grant 16SDG30040000 from the American Heart Association (to T.M.); by National Institutes of Health Grant HL065217, American Heart Association Grant-In-Aid 09GRNT2110159, and a grant from the Jerome Lejeune Foundation (all to J.P.K.); by a PhD Fellowship from the Spanish Ministry of Economy and Competitiveness (BES-2014-068464 and EEBB-I-16-11189) (to P.G-M) and by grants from the Spanish Ministry of Economy and Competitiveness (BFU2010-17857 and BFU2013-47531-R) and by a grant on rare diseases from the Basque Foundation for Health Innovation and Research, BIOEF, and funds raised by EITB Maratoia 2015 (all to L.A.M.-C).

Acknowledgements

We thank Dr. Adriana Rojas for maintenance of our X-Ray equipment and for valuable support and technical assistance during data collection. We also thank the staff at beamlines ID23.1 and ID29 of the European Synchrotron Radiation Facility and the staff at BL13 XALOC beamline of ALBA synchrotron facility for valuable support and technical assistance during synchrotron data collection. This work was supported by the Scientist Development Grant 16SDG30040000 from the American Heart Association (to T.M.); by National Institutes of Health Grant HL065217, American Heart Association Grant-In-Aid 09GRNT2110159, and a grant from the Jerome Lejeune Foundation (all to J.P.K.); by a PhD Fellowship from the Spanish Ministry of Economy and Competitiveness (BES-2014-068464 and EEBB-I-16-11189) (to P.G-M) and by grants from the Spanish Ministry of Economy and Competitiveness (BFU2010-17857 and BFU2013-47531-R) (all to L.A.M.-C). We thank MINECO for the Severo Ochoa Excellence Accreditation (SEV-2016-0644).

Appendix A. Supplementary data

Supplementary data associated with this article can be found, in the online version, at http://dx.doi.org/10.1016/j.jsb.2017.12.008.

References

Adams, P.D., Afonine, P.V., Bunkóczi, G., Chen, V.B., Davis, I.W., Echols, N., Headd, J.J., Hung, L.W., Kapral, G.J., Grosse-Kunstleve, R.W., McCoy, A.J., Moriarty, N.W., Oeffner, R., Read, R.J., Richardson, D.C., Richardson, J.S., Terwilliger, T.C., Zwart, P.H., 2010. PHENIX: a comprehensive Python-based system for macromolecular structure solution. Acta Crystallogr. D Biol. Crystallogr. 66 (2), 213–221.

Alcaide, P., Krijt, J., Ruiz-Sala, P., Ješina, P., Ugarte, M., Kožich, V., Merinero, B., 2015. Enzymatic diagnosis of homocystinuria by determination of cystathionine-ß-synthase activity in plasma using LC-MS/MS. Clin. Chim. Acta 438, 261–265.

Anashkin, V.A., Baykov, A.A., Lahti, R., 2017. Enzymes regulated via cystathionine β-synthase domains. Biochemistry (Mosc) 82 (10), 1079–1087. http://dx.doi.org/10.1134/S0006297917100017.

Auger, S., Yuen, W.H., Danchin, A., Martin-Verstraete, I., 2002. The metIC operon involved in methionine biosynthesis in *Bacillus subtilis* is controlled by transcription antitermination. Microbiology 148, 507–518.

Bateman, A., 1997. The structure of a domain common to archaebacteria and the homocystinuria disease protein. Trends. Biochem. Sci. 22 (1), 12–13.

Banerjee, R., Evande, R., Kabil, O., Ojha, S., Taoka, S., 2003. Reaction mechanism and regulation of cystathionine β-synthase. Biochim. Biophys. Acta 1647 (1–2), 30–35.

Baykov, A.A., Tuominen, H.K., Lahti, R., 2011. The CBS domain: A protein module with an emerging prominent role in regulation. ACS Chem. Biol. 6 (11), 1156–1163.

Beatty, P.W., Reed, D.J., 1980. Involvement of the cystathionine pathway in the biosynthesis of glutathione by isolated rat hepatocytes. Arch. Biochem. Biophys. 204, 80–87.

Bermúdez, M., Frank, N., Bernal, J., Urreizti, R., Briceño, I., Merinero, B., Perez-Cerdá, C., Ugarte, M., Grinberg, D., Balcells, S., Kraus, J.P., 2006. High prevalence of CBS p. T191M mutation in homocystinuric patients from Colombia. Hum. Mutat. 27 (3), 296.

Beyer, K., Lao, J.I., Carrato, C., Rodriguez-Vila, A., Latorre, P., Mataró, M., Llopis, M.A., Mate, J.L., Ariza, A., 2004. Cystathionine β-synthase as a risk factor for Alzheimer disease. Curr. Alzheimer Res. 1 (2), 127–133.

Brosnan, J.T., Brosnan, M.E., 2006. The sulfur-containing amino acids: an overview. J. Nutr. 136, 1636S–1640S.

Carmel, R., Jacobsen, D.W., 2001. Homocysteine in Health and Disease, first ed. Cambridge University Press, Cambridge.

Cherest, H., Surdin-Kerjan, Y., 1992. Genetic analysis of a new mutation conferring cysteine auxotrophy in Saccharomyces cerevisiae: updating of the sulfur metabolism pathway. Genetics 130, 51–58.

Christen, P., Mehta, P.K., 2001. From cofactor to enzymes. The molecular evolution of pyridoxal-5′-phosphate-dependent enzymes. Chem. Rec. 1 (6), 436–447.

De Lucca, M., Casique, L., 2004. Characterization of cystathionine β-synthase synthase gene mutations in homocystinuric Venezuelan patients: identification of one novel mutation in exon 6. Mol. Genet. Metab. 81 (3), 209–215.

Devi, S., Abdul Rehman, S.A., Tarique, K.F., Gourinath, S., 2017. Structural characterization and functional analysis of cystathionine β-synthase: an enzyme involved in the reverse transsulfuration pathway of Bacillus anthracis. FEBS J. http://dx.doi.org/10.1111/febs.14273.

Emsley, P., Lohkamp, B., Scott, W.G., Cowtan, K., 2010. Features and development of Coot. Acta Crystallogr. D Biol. Crystallogr. 66, 486–501.

Ereño-Orbea, J., Majtan, T., Oyenarte, I., Kraus, J.P., Martínez-Cruz, L.A., 2013a. Structural basis of regulation and oligomerization of human cystathionine β-synthase synthase, the central enzyme of transsulfuration. Proc. Natl. Acad. Sci. U.S.A. 110, E3790–E3799.

Ereño-Orbea, J., Oyenarte, I., Martínez-Cruz, L.A., 2013b. CBS domains: ligand binding sites and conformational variability. Arch. Biochem. Biophys. 540 (1–2), 70–81.

Ereño-Orbea, J., Majtan, T., Oyenarte, I., Kraus, J.P., Martínez-Cruz, L.A., 2014. Structural insight into the molecular mechanism of allosteric activation of human cystathionine β-synthase synthase by S-adenosylmethionine. Proc. Natl. Acad. Sci. U.S.A. 111, E3845–E3852.

Eto, K., Asada, T., Arima, K., Makifuchi, T., Kimura, H., 2002. Brain hydrogen sulfide is severely decreased in Alzheimer's disease. Biochem. Biophys. Res. Commun. 293 (5), 1485–1488.

Hyde, C.C., Ahmed, S.A., Padlan, E.A., Miles, E.W., Davies, D.R., 1988. Three-dimensional structure of the tryptophan synthase α2 β2 multienzyme complex from Salmonella typhimurium. J. Biol. Chem. 263, 17857–17871.

Hine, C., Harputlugil, E., Zhang, Y., Ruckenstuhl, C., Lee, B.C., Brace, L., Longchamp, A., Trevino-Villarreal, J.H., Mejia, P., Ozaki, C.K., Wang, R., Gladyshev, V.N., Madeo, F., Mair, W.B., Mitchell, J.R., 2015. Endogenous hydrogen sulfide production is essential for dietary restriction benefits. Cell. 160 (1–2), 132–144.

Hnízda, A., Jurga, V., Raková, K., Kožich, V., 2012. Cystathionine β-synthase mutants

exhibit changes in protein unfolding: conformational analysis of misfolded variants in crude cell extracts. J. Inherit. Metab. Dis. http://dx.doi.org/10.1007/s10545-011-9407-4.
Janosík, M., Kery, V., Gaustadnes, M., Maclean, K.N., Kraus, J.P., 2001a. Regulation of human cystathionine β-synthase by S-adenosyl-L-methionine: evidence for two catalytically active conformations involving an autoinhibitory domain in the C-terminal region. Biochemistry 40, 10625–10633.
Janosík, M., Oliveriusova, J., Janosikova, B., Sokolova, J., Kraus, E., Kraus, J.P., Kozich, V., 2001. Impaired heme binding and aggregation of mutant cystathionine β-synthase subunits in homocystinuria. Am. J. Hum. Genet. 68, 1506–1513.
Jhee, K.H., McPhie, P., Miles, E.W., 2000. Domain architecture of the heme-independent yeast cystathionine β-synthase provides insights into mechanisms of catalysis and regulation. Biochemistry 39 (34), 10548–10556.
Kabil, O., Banerjee, R., 1999. Deletion of the regulatory domain in the pyridoxal phosphate-dependent heme protein cystathionine β-synthase alleviates the defect observed in a catalytic site mutant. J. Biol. Chem. 274, 31256–31260.
Kabil, O., Banerjee, R., 2010. Redox biochemistry of hydrogen sulfide. J. Biol. Chem. 285, 21903–21907.
Kabil, H., Kabil, O., Banerjee, R., Harshman, L.G., Pletcher, S.D., 2011. Increased transsulfuration mediates longevity and dietary restriction in *Drosophila*. Proc. Natl. Acad. Sci. U.S.A. 108 (40), 16831–16836.
Kabsch, W., 2010. XDS. Acta Crystallogr. D Biol. Crystallogr. 66, 125–132.
Kamoun, P., 2004. Endogenous production of hydrogen sulfide in mammals. Amino Acids 26 (3), 243–254.
Katsushima, F., Oliveriusova, J., Sakamoto, O., Ohura, T., Kondo, Y., Iinuma, K., Kraus, E., Stouracova, R., Kraus, J.P., 2006. Expression study of mutant cystathionine β-synthase found in Japanese patients with homocystinuria. Mol. Genet. Metab. 87, 323–328.
Kery, V., Poneleit, L., Kraus, J.P., 1998. Trypsin cleavage of human cystathionine β-synthase into an evolutionarily conserved active core: structural and functional consequences. Arch. Biochem. Biophys. 355 (2), 222–232.
Koutmos, M., Kabil, O., Smith, J.L., Banerjee, R., 2010. Structural basis for substrate activation and regulation by cystathionine β-synthase (CBS) domains in cystathionine β-synthase. Proc. Natl. Acad. Sci. U.S.A. 107, 20958–20963.
Kredich, N.M., 1996. Biosynthesis of cysteine. In: Neidhardt, F.C. (Ed.), *Escherichia coli* and *Salmonella*: Cellular and Molecular Biology, second ed. American Society for Microbiology, Washington, DC.
Krissinel, E., Henrick, K., 2007. "Protein interfaces, surfaces and assemblies" service PISA at the European Bioinformatics Institute. Inference of macromolecular assemblies from crystalline state. J. Mol. Biol. 372, 774–797.
Larkin, M.A., Blackshields, G., Brown, N.P., Chenna, R., McGettigan, P.A., McWilliam, H., Valentin, F., Wallace, I.M., Wilm, A., Lopez, R., Thompson, J.D., Gibson, T.J., Higgins, D.G., 2007. Clustal W and Clustal X version 2.0. Bioinformatics 23, 2947–2948.
Macnicol, P.K., Datko, A.H., Giovanelli, J., Mudd, S.H., 1981. Homocysteine biosynthesis in green plants: physiological importance of the transsulfuration pathway in *Lemna paucicostata*. Plant Physiol. 68, 619–625.
Matoba, Y., Yoshida, T., Izuhara-Kihara, H., Noda, M., Sugiyama, M., 2017. Crystallographic and mutational analyses of cystathionine β-synthase in the H2S-synthetic gene cluster in Lactobacillus plantarum. Protein Sci. 26 (4), 763–783.
McCorvie, T.J., Kopec, J., Hyung, S.J., Fitzpatrick, F., Feng, X., Termine, D., Strain-Damerell, C., Vollmar, M., Fleming, J., Janz, J.M., Bulawa, C., Yue, W.W., 2014. Inter-domain communication of human cystathionine β-synthase: structural basis of S-adenosyl-L-methionine activation. J. Biol. Chem. 289 (52), 36018–36030.
Majtan, T., Singh, L.R., Wang, L., Kruger, W.D., Kraus, J.P., 2008. Active cystathionine β-synthase can be expressed in heme-free systems in the presence of metal-substituted porphyrins or a chemical chaperone. J. Biol. Chem. 283, 34588–34595.
Majtan, T., Liu, L., Carpenter, J.F., Kraus, J.P., 2010. Rescue of cystathionine β-synthase (CBS) mutants with chemical chaperones: purification and characterization of eight CBS mutant enzymes. J. Biol. Chem. 285, 15866–15873.
Majtan, T., Pey, A.L., Fernández, R., Fernández, J.A., Martínez-Cruz, L.A., Kraus, J.P., 2014. Domain organization, catalysis and regulation of eukaryotic cystathionine β-synthases. PLoS One 9 (8), e105290.
Meier, M., Janosík, M., Kery, V., Kraus, J.P., Burkhard, P., 2001. Structure of human cystathionine β-synthase: a unique pyridoxal 5'-phosphate-dependent heme protein. EMBO J. 20, 3910–3916.
Meier, M., Oliveriusova, J., Kraus, J.P., Burkhard, P., 2003. Structural insights into mutations of cystathionine β-synthase. Biochim. Biophys. Acta 1647 (1–2), 206–213.
Miles, E.W., Kraus, J.P., 2004. Cystathionine β-synthase: structure, function, regulation, and location of homocystinuria-causing mutations. J. Biol. Chem. 279, 29871–29874.
Mudd, S.H., Finkelstein, J.D., Irreverre, F., Laster, L., 1965. Transsulfuration in mammals. Microassays and tissue distributions of three enzymes of the pathway. J Biol. Chem. 240 (11), 4382–4392.
Mudd, S.H., Havlik, R., Levy, H.L., McKusick, V.A., Feinleib, M., 1982. Cardiovascular risk in heterozygotes for homocystinuria. Am. J. Hum. Genet. 34, 1018–1021.
Mudd, S.H., Levy, H.L., Kraus, J.P., 2001. Disorders of transsulfuration, 8th ed. McGraw-Hill, New York, pp. 2007–2056.
Mudd, S.H., 2011. Hypermethioninemias of genetic and non-genetic origin: A review. Am. J. Med. Genet. C Semin. Med. Genet. 157C (1), 3–32.
Murshudov, G.N., Skubák, P., Lebedev, A.A., Pannu, N.S., Steiner, R.A., Nicholls, R.A., Winn, M.D., Long, F., Vagin, A.A., 2011. REFMAC5 for the refinement of macromolecular crystal structures. Acta Crystallogr. D Biol. Crystallogr. 67, 355–367.
Oyenarte, I., Majtan, T., Ereño, J., Corral-Rodríguez, M.A., Klauduiny, J., Majtan, J., Kraus, J.P., Martínez-Cruz, L.A., 2012. Purification, crystallization and preliminary crystallographic analysis of the full-length cystathionine β-synthase from *Apis mellifera*. Acta Crystallogr. Sect. F Struct. Biol. Cryst. Commun. 68 (Pt 11), 1323–1328.
Otwinowski, Z., Minor, W., 1997. Processing of X-ray diffraction data collected in oscillation mode. Methods Enzymol. 276, 307–326.
Parry-Smith, D.J., Payne, A.W., Michie, A.D., Attwood, T.K., 1998. CINEMA-a novel colour interactive editor for multiple alignments. Gene 221 (1) GC57-63.
Paul, B.D., Snyder, S.H., 2012. H_2S signalling through protein sulfhydration and beyond. Nat. Rev. Mol. Cell Biol. 13 (8), 499–507.
Pettersen, E.F., Goddard, T.D., Huang, C.C., Couch, G.S., Greenblatt, D.M., Meng, E.C., Ferrin, T.E., 2004. UCSF Chimera -a visualization system for exploratory research and analysis. J. Comput. Chem. 25 (13), 1605–1612.
Porto, M.P., Galdieri, L.C., Pereira, V.G., Vergani, N., da Rocha, J.C., Micheletti, C., Martins, A.M., Perez, A.B., Almeida, V.D., 2005. Molecular analysis of homocystinuria in Brazilian patients. Clin. Chim. Acta 362, 71–78.
Prudova, A., Bauman, Z., Braun, A., Vitvitsky, V., Lu, S.C., Banerjee, R., 2006. S-adenosylmethionine stabilizes cystathionine β-synthase and modulates redox capacity. Proc. Natl. Acad. Sci. USA 103 (17), 6489–6494.
Raj, I., Mazumder, M., Gourinath, S., 2013. Molecular basis of ligand recognition by OASS from *E. histolytica*: insights from structural and molecular dynamics simulation studies. Biochim. Biophys. Acta 1830, 4573–4583.
Rhee, S., Parris, K.D., Ahmed, S.A., Miles, E.W., Davies, D.R., 1996. Exchange of K+ or Cs+ for Na+ induces local and long-range changes in the three-dimensional structure of the tryptophan synthase α2β2 complex. Biochemistry 35 (13), 4211–4221.
Seshadri, S., Beiser, A., Selhub, J., Jacques, P.F., Rosenberg, I.H., D'Agostino, R.B., Wilson, P.W., Wolf, P.A., 2002. Plasma homocysteine as a risk factor for dementia and Alzheimer's disease. N. Engl. J. Med. 346, 476–483.
Shatalin, K., Shatalina, E., Mironov, A., Nudler, E., 2011. H_2S: a universal defense against antibiotics in bacteria. Science 334 (6058), 986–990.
Singh, S., Madzelan, P., Banerjee, R., 2007. Properties of an unusual heme cofactor in PLP-dependent cystathionine β-synthase. Nat. Prod. Rep. 24 (3), 631–639.
Singh, S., Padovani, D., Leslie, R.A., Chiku, T., Banerjee, R., 2009. Relative contributions of cystathionine β-synthase and γ-cystathionase to H2S biogenesis via alternative trans-sulfuration reactions. J. Biol. Chem. 284 (33), 22457–22466.
Singh, S., Banerjee, R., 2011. PLP-dependent H_2S biogenesis. Biochim. Biophys. Acta 1814 (11), 1518–1527.
Singh, S., Ballou, D.P., Banerjee, R., 2011. Pre-steady-state kinetic analysis of enzyme-monitored turnover during cystathionine β-synthase-catalyzed H_2S generation. Biochemistry 50 (3), 419–425.
Stipanuk, M.H., 1986. Metabolism of sulfur-containing amino acids. Annu. Rev. Nutr. 6, 179–209.
Szabó, C., 2007. Hydrogen sulphide and its therapeutic potential. Nat. Rev. Drug Discov. 6 (11), 917–935.
Taoka, S., Lepore, B.W., Kabil, O., Ojha, S., Ringe, D., Banerjee, R., 2002. Human cystathionine β-synthase is a heme sensor protein. Evidence that the redox sensor is heme and not the vicinal cysteines in the CXXC motif seen in the crystal structure of the truncated enzyme. Biochemistry 41, 10454–10461.
Taoka, S., Banerjee, R., 2002. Stopped-flow kinetic analysis of the reaction catalyzed by the full-length yeast cystathionine β-synthase. J. Biol. Chem. 277 (25), 22421–22425.
Urreizti, R., Balcells, S., Rodés, M., Vilarinho, L., Baldellou, A., Couce, M.L., Muñoz, C., Campistol, J., Pintó, X., Vilaseca, M.A., Grinberg, D., 2003. Spectrum of CBS mutations in 16 homocystinuric patients from the Iberian Peninsula: high prevalence of T191M and absence of I278T or G307S. Hum. Mutat. 22 (1), 103.
Urreizti, R., Asteggiano, C., Cozar, M., Frank, N., Vilaseca, M.A., Grinberg, D., Balcells, S., 2006a. Functional assays testing pathogenicity of 14 cystathionine β-synthase mutations. Hum. Mutat. 27, 211.
Urreizti, R., Asteggiano, C., Bermúdez, M., Córdoba, A., Szlago, M., Grosso, C., de Kremer, R.D., Vilarinho, L., D'Almeida, V., Martínez-Pardo, M., Peña-Quintana, L., Dalmau, J., Bernal, J., Briceño, I., Couce, M.L., Rodés, M., Vilaseca, M.A., Balcells, S., Grinberg, D., 2006b. The p. T191M mutation of the CBS gene is highly prevalent among homocystinuric patients from Spain, Portugal and South America. J. Hum. Genet. 51, 305–313.
Vozdek, R., Hnízda, A., Krijt, J., Kostrouchová, M., Kožich, V., 2012. Novel structural arrangement of nematode cystathionine β-synthases: characterization of *Caenorhabditis elegans* CBS-1. Biochem. J. 443 (2), 535–547.
Yadav, P.K., Banerjee, R., 2012. Detection of reaction intermediates during human cystathionine β-synthase-monitored turnover and H_2S production. J. Biol. Chem. 287 (52), 43464–43471.
Weeks, C.L., Singh, S., Madzelan, P., Banerjee, R., Spiro, T.G., 2009. Heme regulation of human cystathionine β-synthase activity: Insights from fluorescence and Raman spectroscopy. J. Am. Chem. Soc. 131, 12809–12816.
Welch, G.N., Loscalzo, J., 1998. Homocysteine and atherothrombosis. N. Engl. J. Med. 338, 1042–1050.
Winn, M.D., Murshudov, G.N., Papiz, M.Z., 2003. Macromolecular TLS refinement in REFMAC at moderate resolutions. Methods Enzymol. 374, 300–321.